Journal of Solid State Electrochemistry (2025) 29:2101–2106
https://doi.org/10.1007/s10008-025-06247-8

SHORT COMMUNICATION

The dissolution and precipitation kinetics of solid particles: the influence of adsorption

Jake M. Yang[1] · **Richard G. Compton**[2,3]

Received: 21 January 2025 / Revised: 24 February 2025 / Accepted: 24 February 2025 / Published online: 5 March 2025

Abstract

The dissolution or growth of solid particles, analogous to electro-dissolution and deposition processes, can occur either under mass transport or surface kinetic control with the latter considered increasingly likely as the size of the particle decreases since the rate of diffusion scales inversely with particle size. The conditions under which these processes are influenced by the adsorption of species onto the dissolving or growing surface are explored both generically and illustrated by the specific case of calcite ($CaCO_3$) particle formation/dissolution in aqueous solution forming or from the component ions. Under surface control, the presence of adsorbed species leads to 'blocking' of the reactive surface, and a corresponding reduction in the observed rate. Under mass transport control, the concentrations of the various species in the layer of solution next to the solid are in equilibrium with the solid. They are thus pinned by the pertinent solubility product coupled with the solute fluxes in and out of the diffusion layer. In this situation, adsorption effects on the kinetics of dissolution/growth emerge in the observed *effective* thermodynamic solubility product as inferred from experiment. The predictions for the reduction in the rate of calcite dissolution in aqueous solution in the presence of dissolved Mg^{2+} cations are in quantitative agreement with experiment suggesting that for solids such as calcium carbonate, the effective solubility product and hence dissolution or precipitation rate is generically dependent on the identity and coverage of the adsorbate.

Background

The kinetics of precipitation and dissolution fundamentally and profoundly influence a vast diversity of processes not least in respect of both the environment and chemical technology including the mineral mining and processing industry [1–5]. The inherently two-phase nature of the growth/dissolution of solids in a liquid phase implies that the processes are, intrinsically, at least a two-step reaction, involving both the transport of solute to or from the bulk phase to the growing interface and also integration/detachment of material at the interface into or from the solid. Either of these two steps can be rate-determining.

✉ Richard G. Compton
richard.compton@chem.ox.ac.uk

[1] Centre for Sustainable Materials Processing, School of Chemistry, University of Leicester, Leicester LE1 7RH, Great Britain

[2] St John's College, St Giles, Oxford OX1 3JP, Oxford, Great Britain

[3] Department of Chemistry, Physical and Theoretical Chemistry Laboratory, University of Oxford, South Parks Road, Oxford, Great Britain

The aforementioned two-step processes underpinning all precipitation or dissolution reactions (see footnote) are also commonly seen and studied in electrochemistry. In electrochemistry, the interfacial kinetics can be controlled by the magnitude of the thermodynamic driving force in the form of the applied electrode potential [6]. At sufficiently high applied over-potentials, it is well known that the mass-transport limited flux (mol m^2 s^{-1}) to smaller electrode particles is greater than that of larger electrodes [7]. Similarly, it is well appreciated that, for particles undergoing precipitation or dissolution, the diffusive transport fluxes to smaller particles are greater than fluxes to larger ones. In other words, for a sufficiently small particle, the rate-determining step must become the surface-controlled reaction whilst transport control will be exerted for large enough particles [8]. This, for example, explains why silver nanoparticles are more toxic than bulk silver [9, 10].

This work, inspired by electrochemistry and driven by the need to understand calcite precipitation or dissolution kinetics in the world's oceans, explores the influence of adsorption and the effect of particle size on the rate of precipitation or dissolution. The world's oceans contain, for example, high concentrations of Mg^{2+} (*ca.* 55 mM) which is known to be a

calcite dissolution inhibitor [11–14]. First, we discuss reactions with a stoichiometry ratio between moles of reactants and moles of products of 1:1 before moving to discuss how this affects a more complex reaction with stoichiometry of 1:2 such as in the case of $CaCO_3$(s) in which dissolution produces for example cations and anions so that there is a change in the number of moles between reactants and products.

Main text

First, we explore the consequences of surface adsorption on both surface kinetic and mass transport control of the reaction rate with respect to the dissolution or precipitation of solid particles of species Z, on which adsorption of a surface-active species, X, takes place:

$$X(aq) \underset{k_{des}}{\overset{k_{ads}}{\rightleftharpoons}} X(ads) \tag{1}$$

The simplest case is that of Langmuirian adsorption [15, 16]. If k_{ads} (m s^{-1}) is the rate constant for adsorption of X and k_{des} (mol m^{-2} s^{-1}) is that for desorption, then the ratio k_{ads}/k_{des} is equal to K, where K is a pressure and temperature-dependent equilibrium constant for adsorption with units of reciprocal concentration. The fractional coverage, Θ, of the surface of Z covered with X is given by

$$\Theta = \frac{K[X]}{1 + K[X]} \tag{2}$$

and $0 < \Theta < 1$.

The two limiting kinetic cases identified above in the absence of adsorption are characterised by the following simple scheme written for the case of dissolution:

$$Z(s) \underset{k_b}{\overset{k_f}{\rightleftharpoons}} Z(aq) \overset{k_{MT}}{\rightarrow} bulk \tag{3}$$

where k_f is the rate constant for dissolution with units of flux (mol m^{-2} s^{-1}) and k_b is that for precipitation (m s^{-1}). k_{MT} is the rate constant for mass transport which for a spherical particle, of radius r, experiencing diffusion-only mass transport in bulk solution is given by $k_{MT} = D/r$ where D is the diffusion coefficient of the dissolved Z. Analogous expressions are available for a spherical particle supported on an insulating plane [17] and for a cube [18, 19]. Consideration of steady-state kinetics in respect of (3) leads to the following expression for the overall flux J (mol m^{-2} s^{-1}):

$$flux\ J = [Z]_{surface} k_{MT} = \frac{k_f k_{MT}}{k_b + k_{MT}} \tag{4}$$

As illustrated in Fig. 1, for surface control where $k_{MT} \gg k_f \& k_b$ the above expression readily becomes

$$J = k_f \tag{5}$$

whilst for mass transport control dissolution ($k_{MT} \ll k_f, k_b$), flux becomes

$$J = K^o_{sp} k_{MT} \tag{6}$$

where the solubility product $K^o_{sp} = [Z]_{surface} = k_f/k_b$ and where the subscript 'surface' indicates the equilibrium concentration adjacent to the solid surface and the superscript 'o' denotes standard conditions and the absence of adsorption.

In the two limits, the fluxes calculated via either (5) or (6) can be linked with the gain or loss of material by the solid and hence, via the known density of the solid, its change in size as a function of time. This leads to a simple yet powerful method for distinguishing between two limiting kinetic cases [20–22]. For surface control, the change in radius, r, for a spherical particle, or the length of a quasi-cubic crystal in the case of calcite, is linear in time, so that dr/dt (or dl/dt in the case of a cubic particle) is a constant whereas for mass transport control the two-dimensional projection area, A, changes linearly with time [20–22]. In the latter case, dA/dt is constant. Thus, for particles of a few microns in size observation via optical microscopy of the change in dimensions of the growth or dissolving solid particle allows the mechanism to be characterised. By linking size change to the change in the amount of solid, either a surface rate constant or a solubility product can be inferred [20, 21].

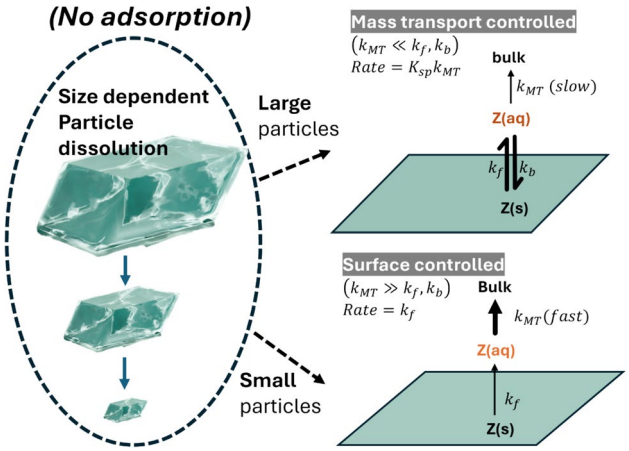

Fig. 1 A schematic diagram illustrating the size-dependent effect on the rate-determining step for particles undergoing dissolution. The stoichiometry of the illustrated dissolution process is 1:1, i.e. $Z(s) \rightarrow Z(aq)$. For large particles the mass transport coefficient, k_{MT}, is slow and rate-determining. On the other hand, the mass transport coefficient, k_{MT}, is large for small particles so the surface kinetics (k_f and k_b) becomes rate-determining

These considerations relate to the simple case where the solid is comprised of molecules of Z which equilibrate with Z in solution. In the case of an ionic solid such as calcium carbonate, the thermodynamically most stable form of which is calcite, the pertinent equilibrium is

$$CaCO_3(s) \underset{k_b}{\overset{k_f}{\rightleftharpoons}} Ca^{2+}(aq) + {CO_3}^{2-}(aq) \overset{k_{MT}}{\rightarrow} bulk \tag{7}$$

where k_b has units of $mol^{-1}\ m^4\ s^{-1}$. In this case, the thermodynamic solubility constant, K^o_{sp}, also referred to as the *stoichiometric* solubility constant in seawater studies, equals the product of the relevant free ions

$$K^o_{sp} = [Ca^{2+}][{CO_3}^{2-}] \tag{8}$$

In the hypothetical absence of any homogeneous chemical reactions of the dissolved ions, the flux under mass transport control is given by

$$J = {K^0_{sp}}^{1/2} k_{MT} \tag{9}$$

where k_{MT} is again given by D/r but now reflects an average diffusion coefficient for the two ions Ca^{2+} and ${CO_3}^{2-}$, the diffusion coefficients of the two ions being in any case rather close in value ($D_{Ca^{2+}} = 7.92 \times 10^{-10}$ and $D_{{CO_3}^{2-}} = 9.23 \times 10^{-10}\ m^2\ s^{-1}$ at 25 °C) [23]. However, in reality, the dissolved ions participate in a plurality of chemical reactions including with water forming bicarbonate ions (and at low pH, carbonic acid and hence dissolved CO_2), and with each other forming $CaCO_3$ ion pairs in pure water. Moreover, a plurality of ion pairs is observed in complex media such as seawater (with an ionic strength of *ca.* 0.7 M) [24–26]. Under these conditions and assuming all Ca^{2+} species formed are in equilibrium with their component ions, then the *dissolution* flux becomes

$$J = k_{MT} \sum \left[Ca^{2+}\right]_{surface} \tag{10}$$

where the summation is over all the Ca^{2+} species. In this case, if the homogeneous chemistry is understood and the relevant equilibrium constants known [24], then it is possible to use microscopic sizing measurements to infer that thermodynamic control exists (from the constancy of the rate of change of projected area with time, $dA\ /\ dt$), or not. It is also possible to obtain a measurement of the thermodynamic solubility product, as defined above in terms of the concentrations of the free ions.

The accepted value of K^o_{sp} for calcite in pure water is reported as $3.3 \times 10^{-9}\ M^2$ [27]. Note that this is (significantly) different from the ***apparent*** stoichiometric solubility product used widely to describe solubility in seawater which is defined as [28, 29].

$$K^o_{sp,\ apparent} = \sum [Ca^{2+}] \sum [{CO_3}^{2-}] \tag{11}$$

In this equation, the summations extend over all Ca^{2+} and CO_3^{2-} containing species. Note that both K^o_{sp} and $K^o_{sp,\ apparent}$ are written, following usual practice [30], in terms of concentrations rather than activities so are ionic strength dependent.

The above shows that a combination of measurements of particle size coupled with the modelling of the relevant solution phase chemical equilibria allows the inference of the thermodynamic solubility product defined in terms of the free ion concentrations. This in turn allows the investigation as to whether the presence of adsorbed species can alter the value of K^o_{sp}. Considering first the dissolution of Z as introduced above the presence of an adsorbate of coverage Θ, we note the expectation that both the forward and back rate constants, k_f and k_b are reduced by the same factor $(1 - \Theta)$ in the presence of adsorption. This is because for the dissolution this factor represents the fraction of exposed surface available from which loss of Z can take place via dissolution and similarly the same fraction is available for the reverse process of precipitation as illustrated in Fig. 2. It follows that for surface-controlled dissolution, the rate of dissolution decreases by a factor of $(1 - \Theta)$, as shown in Fig. 2a). Under mass transport control, at first sight, one might predict that there is no kinetic consequence since both k_f and k_b decrease by the same factor so that their ratio, K^o_{sp}, remains unchanged. Thus, in the case of solid Z dissolving to form molecules of Z in solution under mass transport control, the amount of dissolved Z in the interfacial region is, we might (incorrectly) predict, unchanged from that seen in the absence of adsorption. However, returning to (3), we see by equating fluxes of Z in and out of the diffusion layer that

$$(1 - \Theta)\left\{k_f - k_b[Z]_{aq}\right\} = k_{MT}[Z]_{aq} \tag{12}$$

where the left-hand term reflects the net flux into the diffusion layer and the right-hand term is the flux out of the diffusion layer due to diffusion. It follows that the amount of Z in the diffusion layer is reduced by a factor of $(1 - \Theta)$ since the amount in a steady state is reduced by that factor and hence the appropriate form of (6) in the presence of adsorption is

$$J = (1 - \Theta)K^o_{sp}k_{MT} \tag{13}$$

In physical terms, the diffusional overlap of material being 'injected' into the diffusion layer takes place, as shown on the right-hand side of Fig. 2b), leading to an ever-decreasing average concentration as the coverage, Θ, increases whilst the mass transport coefficient for the diffusion of Z out of the diffusion layer, k_{MT}, remains unchanged. Note that the dissolution from the surface into the diffusion

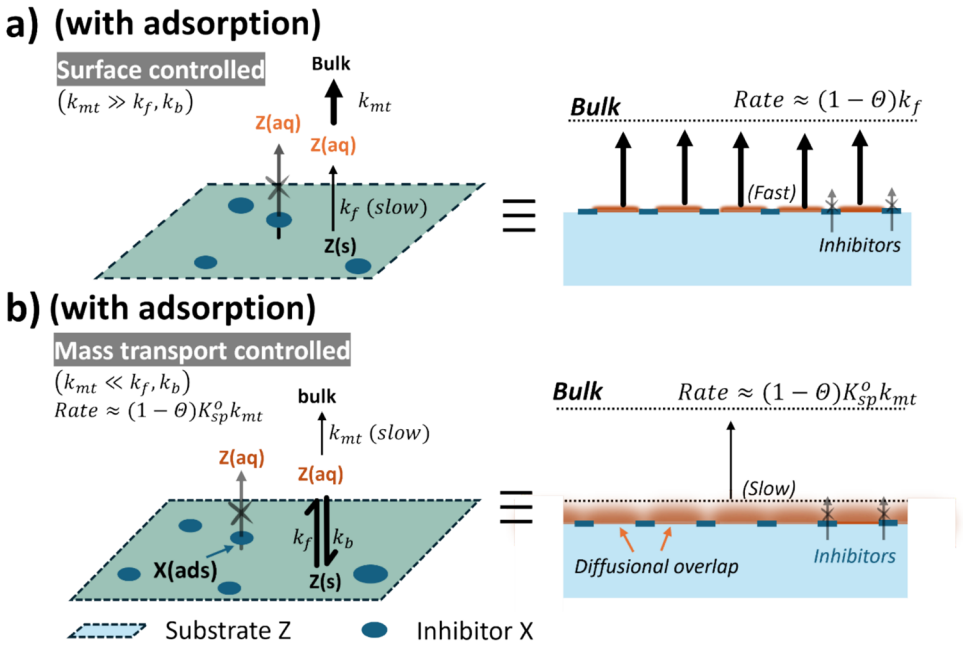

Fig. 2 A schematic diagram showing the dissolution of a solid particle of Z in the presence of an inhibitor, $X(ads)$, adsorbed with a non-zero surface coverage ($0 < \Theta < 1$). Dissolution only occurs on pristine surfaces, absent of the adsorbate, X(ads). The stoichiometry of the dissolution process is 1:1, i.e. $Z(s) \rightarrow Z(aq)$. In the case of surface-controlled dissolution ($k_{MT} \gg k_f,\ k_b$), as shown in (a), the dissolution rate is reduced by a factor that is equal to the fraction of the pristine surface ($1 - \Theta$). In the case of a mass-transport controlled dissolution ($k_{MT} \ll k_f,\ k_b$), the overall rate of dissolution is limited by the rate of mass transport of Z(aq) away from the diffusive layer

layer is spatially heterogeneous because of the adsorbed species partially blocking the process. However, the latter are of atomic or molecular dimensions so the lateral scale of the distance between the points of 'injection' is tiny compared to the physical thickness of the diffusion layer (typically tens or hundreds of microns). Consequentially, lateral diffusion homogenises the concentration of dissolved species within the diffusion layer allowing analysis in terms of the one-dimensional formulation of (3).

We next turn to consider the dissolution of $CaCO_3$ in the presence of an inhibitor. Again, in the surface-controlled regime, it is expected that the dissolution rate is again reduced by a factor of $(1 - \Theta)$. In the mass transport-controlled regime, the net access to the diffusion layer is again reduced by the factor of $(1 - \Theta)$ so that

$$(1 - \Theta)\left\{k_f - k_b\left[Ca^{2+}\right]\left[CO_3^{2-}\right]\right\} = k_{MT}\sum[Ca^{2+}] \quad (14)$$

This equation again shows reduced material entering the diffusion layer and so implies a rate reduced by a factor of $(1 - \Theta)$. Here we expect that the mass transport out of the diffuse layer is limited by a (geometric) mean diffusion coefficient of the various diffusing species containing Ca^{2+} as inferred from the diffusion coefficients of the free ions in pure water [23].

The above predicts that under both mass transport and surface control, the presence of adsorption reduces the dissolution rate by a factor of $(1 - \Theta)$ with complete surface coverage leading to total inhibition. However, the mechanistic criteria of dr/dt and dA/dt being constant for surface or mass transport control are unchanged as is the size threshold for the transition between the two regimes.

We next compare the above theoretical predictions with experiment and consider the dissolution of calcite particles in aqueous solution containing various amounts of dissolved Mg^{2+} ions which are known to slow the dissolution of calcite [14, 31, 32]. In particular, previous reports [20, 22] have shown that the dissolution of micron-sized crystals (and larger) occurs under apparent thermodynamic control, however, at a rate significantly lower than expected from (10) and the known solubility product of calcite [20]. The data were consistent with pinned concentrations of the dissolved ions in the diffusion layer suggesting a possible thermodynamic control. The magnitude of the dissolution fluxes enabled the inference of the product $[Ca^{2+}][CO_3^{2-}]$. This differed from the known true thermodynamic solubility product by a factor of $1/\left\{1 + K_{Mg}[Mg^{2+}]\right\}$ over a wide range of Mg^{2+} concentrations (0–15 mM). This factor corresponds to $(1 - \Theta)$ as predicted by (3) and as shown in Fig. 3.

The above gives a theoretical basis for the observed kinetics of dissolution of solids in the presence of adsorption. Because of the competing fluxes into and out of the diffusion layer under the control of mass transport, the observed rate is predicted for the known thermodynamic solubility product but with a magnitude reduced by a factor of $(1 - \Theta)$. Note that the true thermodynamic solubility product is unchanged and given by k_f/k_b; the reduction is a consequence of the operation of steady-state kinetics controlling the population of dissolved ions in the diffusion layer. For this reason, the dissolution is probably better described as being under

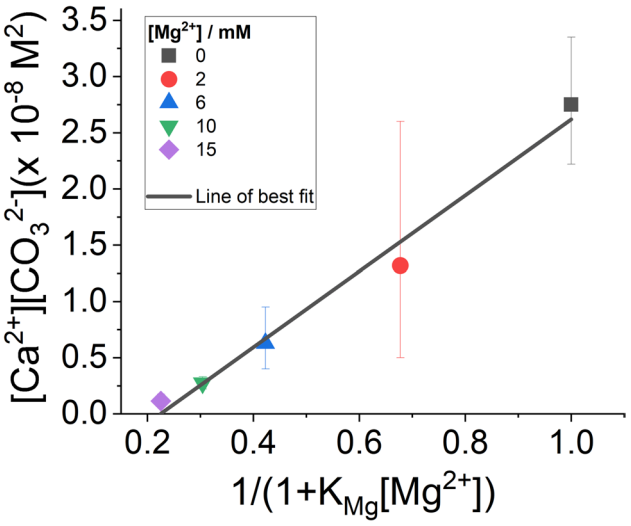

Fig. 3 Plot of $[Ca^{2+}]$ $[CO_3^{2-}]$ inferred from single particle dissolution measurements against $\left(\frac{1}{1+K_{Mg}[Mg^{2+}]}\right)$ The data shown in this figure were obtained from recently published work [20]. The concentration of magnesium ranges from 0 to 15 mM. These dissolution experiments were conducted at ambient laboratory temperature and in aqueous solutions with an ionic strength of 0.3M via the addition of an inert salt, KNO_3. The slope of the linear fit line is 3.4 (± 0.25) x 10^{-8} mol^2 dm^{-6}, Pearson's $r = 0.991$. In terms of the significance of Pearson's r values, a value of 1 means a perfect positive correlation between the model and observations and a r value of 0 means no linear dependency between the model and observations

mass transport control rather than thermodynamic control although the influence of the solubility product, K_{sp}, is clear. Note also that, the rate of dissolution of coccoliths ($CaCO_3$ biomineralized by phytoplankton) show excellent agreement with that of similarly sized pure, laboratory grown calcite over concentrations of Mg^{2+} relevant to the ocean[4].

Conclusions

This work suggests that the reduction in rates of dissolution (and precipitation) as a result of surface adsorption reflects the fraction of the surface not covered with adsorbate regardless of whether surface or mass transport control operates and whether the transport is diffusive or convective. It likely applies to all solids where the adsorption is strong as in Langmuir adsorption for example. This requirement implies that there is no adsorption/desorption of the adsorbate on the timescale of the dissolution/precipitation. The need for exploring surface adsorption effects in modelling the behaviour of solid particles in ocean and other aqueous chemistry is evident.

References

1. BrbootI MM, Abid BA, Al-ShuwaikI NM (2011) Removal of heavy metals using chemicals precipitation. Eng Technol J 29(3):595–612
2. Rothstein F (2019) Differential precipitation of proteins: science and technology. Protein purification process engineering, CRC Press, pp 115–208
3. Wang LK, Vaccari DA, Li Y, Shammas NK (2005) Chemical precipitation. Springer, In Physicochemical treatment processes, pp 141–197
4. Morton-Collings T, Yang M, Compton RG (2024) Controlling crystallisation and dissolution of biogenic CaCO 3 via dissolved magnesium cations. Environmental Science: Advances 3(3):402–410
5. Han B, Porvali A, Lundström M, Louhi-Kultanen M (2018) Lithium recovery by precipitation from impure solutions–lithium ion battery waste. Chem Eng Technol 41(6):1205–1210
6. Richard G. Compton RG, Sanders GHW, Yan JM (2024) Oxford University Press, Electrode potentials
7. Compton RG, Banks CE (2025) Understanding voltammetry; World Scientific, 4th edn
8. Batchelor-McAuley C, Yang M, Rickaby RE, Compton RG (2022) Calcium carbonate dissolution from the laboratory to the ocean: kinetics and mechanism. Chem Eur J 28(68), e202202290
9. Batchelor-McAuley C, Tschulik K, Neumann CC, Laborda E, Compton RG (2014) Why are silver nanoparticles more toxic than bulk silver? Towards understanding the dissolution and toxicity of silver nanoparticles. Int J Electrochem Sci 9(3):1132–1138
10. Batchelor-McAuley C, Tschulik K, Compton RG (2013) Nanotoxicity—an electrochemist's perspective. Port Electrochim Acta 31:249–256
11. Morse JW, Arvidson RS, Lüttge A (2007) Calcium carbonate formation and dissolution. Chem Rev 107(2):342–381
12. Pan Y, Li Y, Ma Q, He H, Wang S, Sun Z, Cai W-J, Dong B, Di Y, Fu W (2021) The role of Mg^{2+} in inhibiting CaCO3 precipitation from seawater. Mar Chem 237:104036
13. Morse JW, Arvidson RS (2002) The dissolution kinetics of major sedimentary carbonate minerals. Earth Sci Rev 58(1–2):51–84
14. Compton RG, Brown CA (1994) The inhibition of calcite dissolution/precipitation: Mg2+ cations. J Colloid Interface Sci 165(2):445–449
15. Langmuir I (1918) The adsorption of gases on plane surfaces of glass, mica and platinum. J Am Chem Soc 40(9):1361–1403
16. Yang M, Compton RG (2019) Adsorption processes coupled with mass transport at macro-electrodes: new insights from simulation. J Electroanal Chem 836:68–76
17. Bobbert P, Wind M, Vlieger J (1987) Diffusion to a slowly growing truncated sphere on a substrate. Physica A 141(1):58–72

18. Wong R, Batchelor-McAuley C, Yang M, Compton RG (2022) Electrochemical heterogeneity at the nanoscale: diffusion to partially active nanocubes. J Phys Chem Lett 13(33):7689–7693
19. Wong R, Batchelor-McAuley C, Yang M, Compton RG (2021) The steady-state diffusional flux to isolated square cuboids in solution and supported on an inert substrate. J Electroanal Chem 903:115818
20. Yang M, Tan L, Batchelor-McAuley C, Compton RG (2024) The solubility product controls the rate of calcite dissolution in pure water and seawater. Chem Sci 15(7):2464–2472
21. Milner MP, Yang M, Compton RG (2024) Vaterite dissolution: mechanism and kinetics. J Phys Chem C 128:10388–10396
22. Fan X, Batchelor-McAuley C, Yang M, Compton RG (2022) Single calcite particle dissolution kinetics: revealing the influence of mass transport. ACS Measurement Science Au 2(5):422–429
23. Lide DR (2004) CRC handbook of chemistry and physics; CRC press
24. Pytkowicz R, Hawley J (1974) Bicarbonate and carbonate ion-pairs and a model of seawater at 25° C 1. Limnol Oceanogr 19(2):223–234
25. Marcus Y, Hefter G (2006) Ion pairing. Chem Rev 106(11):4585–4621
26. Plummer LN, Busenberg E (1982) The solubilities of calcite, aragonite and vaterite in CO2-H2O solutions between 0 and 90 C, and an evaluation of the aqueous model for the system CaCO3-CO2-H2O. Geochim Cosmochim Acta 46(6):1011–1040
27. Millero FJ (2007) The marine inorganic carbon cycle. Chem Rev 107(2):308–341
28. Morse JW, Mucci A, Millero FJ (1980) The solubility of calcite and aragonite in seawater of 35% salinity at 25 C and atmospheric pressure. Geochim Cosmochim Acta 44(1):85–94
29. Mucci A (1983) The solubility of calcite and aragonite in seawater at various salinities, temperatures, and one atmosphere total pressure. Am J Sci 283(7):780–799
30. Equilibrium Constant. 3.0.1 ed. (2019) International Union of Pure and Applied Chemistry (IUPAC)
31. Arvidson RS, Collier M, Davis KJ, Vinson MD, Amonette JE, Luttge A (2006) Magnesium inhibition of calcite dissolution kinetics. Geochim Cosmochim Acta 70(3):583–594
32. Yang M, Batchelor-McAuley C, Barton S, Rickaby RE, Bouman HA, Compton RG (2021) Opto-electrochemical dissolution reveals coccolith calcium carbonate content. Angew Chem Int Ed 60(38):20999–21006